Available online at https://scilett-fsg.uitm.edu.my/

ISSN: 1675-7785
eISSN: 2682-8626

Science Letters 18(4) 2024, 125-132.

# Optimal Effective Carrier Barrier Height of the AlGaN-based Deep-Ultraviolet Light-Emitting Diode through the Wedge-shaped Electron Blocking Layer

Mohammad Amirul Hairol Aman[1,2], Nurul Fathinah Azrisham[1,2], Ahmad Nadzimuddin Nazmi[1,2] and Ahmad Fakhrurrazi Ahmad Noorden[1,2*]

[1]*Centre for Advanced Optoelectronics Research (CAPTOR), Kulliyyah of Science, International Islamic University Malaysia, 25200 Kuantan, Pahang, Malaysia*
[2]*IIUM Photonics and Quantum Centre (IPQC), Kulliyyah of Science, International Islamic University Malaysia, 25200 Kuantan, Pahang, Malaysia*

ARTICLE INFO

*Article history:*
Received 30 April 2024
Revised 31 August 2024
Accepted 30 September 2024
Online first
Published 28 October 2024

*Keywords:*
Deep-ultraviolet light-emitting diode
Electron blocking layer
Luminescence spectrum
Radiative recombination rates

*DOI:*
10.24191/scl.v18i4.9714

ABSTRACT

This work demonstrates the enhancement of luminescence intensity of aluminium gallium nitride (AlGaN)-based deep-ultraviolet light-emitting diode (DUV-LED) via the wedge-shaped electron blocking layer (W-EBL). The AlGaN-based DUV-LED suffers from low luminescence intensity emitted by the device due to electron overflow and minimal hole injection. Utilising the W-EBL in the epitaxy layers with an optimal effective barrier height structure can reduce the overflowing electron and increase the transportation of hole into the active region. The increment in confinement of carrier in the multiple quantum well (MQW) increased the radiative recombination rates and boosted the luminescence intensity of the DUV-LED by 48%.

## INTRODUCTION

In recent years, the deep-ultraviolet (DUV) light-emitting diodes (LEDs) have emerged as very promising optoelectronics devices used in various applications such as UV curing, water, or air cleaning [1,2], and lithography [3,4]. The DUV-LEDs are great replacements for poisonous mercury lamps and gas lasers, commonly used for UV light in air, water, food purification, and sterilization [5,6]. The DUV-LEDs offer high emission efficiency, minimal heat impact, compact size, and extended operational lifespan

* Corresponding author. *E-mail address*: fakhrurrazi@iium.edu.my

https://doi.org/10.24191/scl.v18i4.9714

compared to mercury lamps in industrial settings [5,6]. DUV LEDs have become recognized as an eco-friendly, safer, and less damaging disinfection technique during the COVID-19 pandemic [7,8].
However, DUV-LEDs encounter some drawbacks in research and development, including challenges in low luminescence intensity, internal quantum efficiency, and external quantum efficiency (EQE) below 20% [9]. The luminous efficiency of AlGaN-based LEDs decreases exponentially as they operate at shorter wavelengths, prompting efforts to enhance the quality of epitaxial growth [5]. DUV-LEDs experience efficiency droop due to electron overflow, inefficient hole injection, Auger effect, and carrier delocalization [10]. GaN-based LEDs are frequently utilized to establish an energy barrier, although the problem of electron overflow can be significant under high injection current conditions [10]. The band bending caused by the polarization field at the interfaces of the final quantum barrier (QB) and electron blocking layers (EBL) can reduce the energy barrier and slow down the injection of holes [10]. Various analysis and bandgap engineering techniques have been utilized to enhance the efficiency of DUV-LEDs, including dopant concentration analysis [11], epitaxy layer thickness analysis [12], and different types of superlattice EBL and heterojunction EBL configurations. Nevertheless, these structures' intricate device physics and carrier transport mechanisms still need to be sufficiently characterized [13].

In this work, three DUV-LEDs with different EBL configurations and five quantum wells were simulated. The three DUV-LED structures were named based on the EBL design, such as N-EBL, C-EBL, and W-EBL, which refer to the absence of the EBL, conventional bulk EBL, and a wedge-shaped EBL, respectively. The epitaxial chip was analyzed through the variation of the aluminum composition of the wedge-shaped EBL. The alteration of aluminium composition affects various material properties and influences the optoelectronics performance of the DUV-LED. The simulation of the DUV-LED was performed using the 1-dimensional Poisson, drift-diffusion, and Schrodinger solver (1D-DDCC) developed by Yuh-Renn Wu [14-16]. The 1D-DDCC utilizes the drift-diffusion model to transport the carrier within the heterostructure of the DUV-LED.

Furthermore, the simulation software employs the Schrodinger equation to consider the quantum effects that occur in the DUV-LED, such as tunneling effects. The analysis of the DUV-LED performances covers several optoelectronic properties, such as the energy band diagram, radiative recombination rates, and luminescence spectrum. Through the W-EBL, the optoelectronics properties of DUV-LED were significantly enhanced, and this research may become a stepping stone in improving the DUV-LED technology.

## METHODOLOGY

### Theory of the carrier transport

The carrier transportation in the DUV-LED structure can be understood through the drift-diffusion model (DDM). The three main components in DDM are current density of carrier equations, continuity equations, and Poisson equation, which can be expressed in equations 1, 2, and 3 as [17], [18]

$$\vec{J}_c = q\mu_c c\vec{E} + qD_c\nabla c \tag{1}$$

$$q\frac{\partial c}{\partial t} = -\nabla \cdot \vec{J}_c - q(R - G) \tag{2}$$

$$\nabla \cdot \left(\varepsilon_0\varepsilon_{st}\vec{E}\right) = q(p - n + p_D - n_A) \tag{3}$$

The terms $c, \vec{J}_c, \mu_c, D_c$ and $\vec{E}$ Refer to the carrier, i.e., (electron and hole), current density, mobility of the carrier, diffusion coefficient, and electric field, respectively. The flow of carrier concentrations

https://doi.org/10.24191/scl.v18i4.9714

concerning time can be described via the continuity equation, which consists of the recombination rate, $R$ and generation rate, $G$. The electron and hole are represented by $n$ and $p$ as described in Fig. 1.

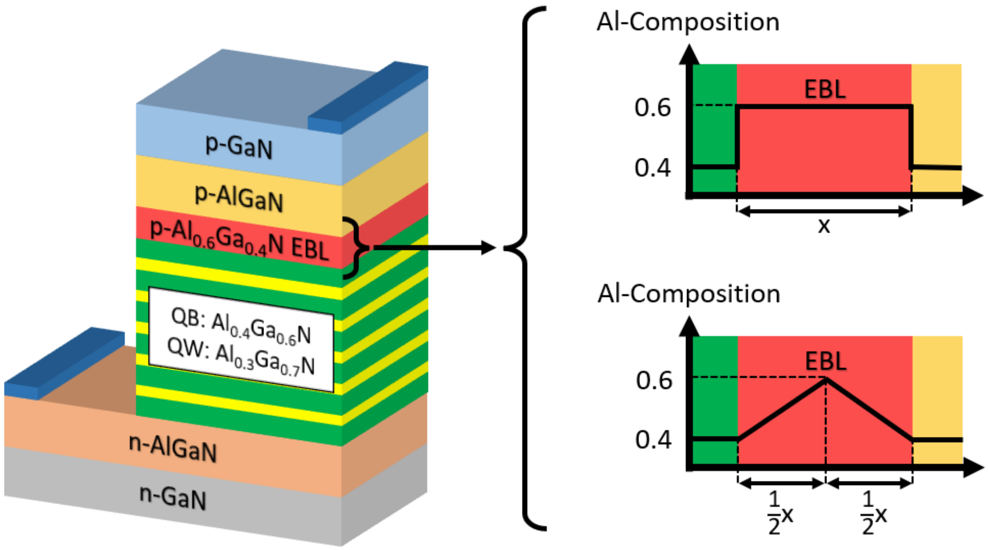


Fig. 1. The schematic diagram of the DUV-LED epitaxial structure. The 36 nm thickness of the EBL is represented by "x".

**DUV-LED configuration**

The epitaxial layer of the DUV-LED consists of gallium nitride (GaN) substrate, followed by n-AlGaN and n-GaN with 0.5 $\mu$m thickness and $5 \times 10^{18}$ cm$^{-3}$ silicon (Si)-doped. The confinement of the carrier in the DUV-LED was achieved through the multiple quantum well (MQW), which consists of five pairs of $Al_{0.3}Ga_{0.7}N$ quantum wells and is alternated with $Al_{0.4}Ga_{0.6}N$ quantum barriers. The thickness of the quantum well and barrier was 3 nm and 12 nm, respectively. The thickness of hole injection layers, p-$Al_{0.4}Ga_{0.6}N$ and p-GaN, was 2.5 $\mu$m. The layers were doped with $5 \times 10^{18}$ cm$^{-3}$ and $1 \times 10^{19}$ cm$^{-3}$ magnesium (Mg)-doped. Bulk p-$Al_{0.6}Ga_{0.4}N$ EBL with a thickness of 36 nm and $1 \times 10^{18}$ cm$^{-3}$ Mg-doped was added to the C-EBL. Meanwhile, the aluminium composition of EBL was altered into a wedge-shaped for W-EBL, as illustrated in Fig. 1. The same thickness and doping were used in the W-EBL and the C-EBL.

## RESULTS AND DISCUSSION

**Energy band diagram**

The optoelectronic properties of the DUV-LED, such as the energy band diagram, radiative recombination rates, and luminescence spectrum, are discussed in this section. The importance of the EBL is highlighted, and a better DUV-LED performance can be achieved through the EBL band-engineering process. Fig. 2 shows the energy band diagram for the N-EBL, C-EBL, and W-EBL, respectively. The dotted line represents the quasi-fermi level, and the solid line represents the bands.

https://doi.org/10.24191/scl.v18i4.9714

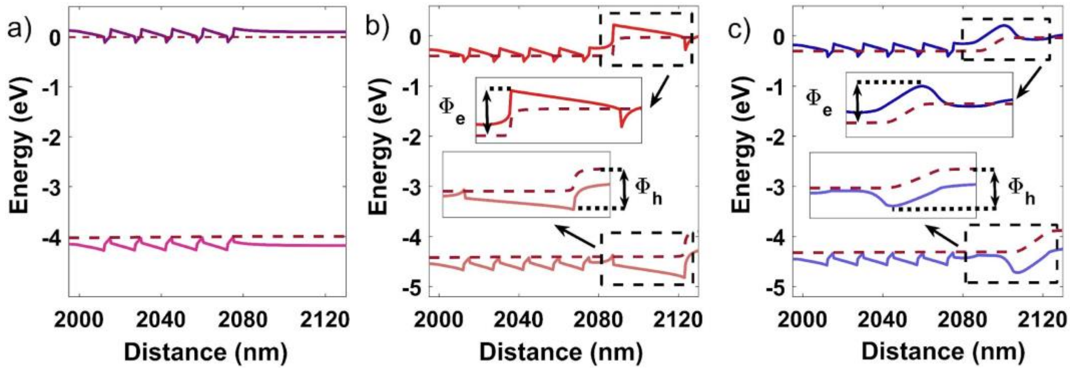


Fig. 2. The energy band diagrams of a) N-EBL, b) C-EBL and W-EBL for the DUV-LED where the $\Phi_e$ and $\Phi_h$ represents the effective barrier height of electron and hole, respectively.

Based on Fig. 2a), there is a flat line in the energy band diagram of the conduction and valance bands for the N-EBL. Contrarily, in Figures 2b) and 2c), trapezoidal and wedge shapes are present in the EBL region of the conduction band and valance bands. The addition of the EBL in the DUV-LED epilayer is performed to reduce electron leakage and improve the injection of the hole into the active region [19]. The EBL creates an effective barrier height for the electron, which blocks the spill-over from the active region into the p-region [20]. The confinement of the electrons in the active region is enhanced and boosts the performance of the DUV-LED. The effective barrier height for electron, $\Phi_e$ , which is measured from the difference between the highest point of the conduction band in the EBL region and the quasi-fermi level immediately before the EBL region [21]. The effective barrier height of the electron for N-EBL, C-EBL, and W-EBL are 0 meV, 618 meV, and 509 mV.

Although the effective barrier height of the electron for C-EBL is higher than W-EBL, due to the grading of the Aluminium composition, the leakage of the electron is still more severe in C-EBL because of the quantum tunneling effect. The transportation of electrons in the epilayer of the DUV-LED is via two methods: (1) thermionic emission [22] and (2) quantum tunneling [17]. The thermionic emission depends on the effective barrier height [22]. In contrast, quantum tunneling depends on the space required to penetrate [17]. The grading of the Aluminium composition in the W-EBL creates a larger space for the electron to penetrate, reducing the electron's leakage and improving the electron's confinement.

In addition, hole transportation into the active region has also been improved via implementing the EBL. The effective barrier height for the hole is measured from the difference between the lowest point of the valance band in the EBL region and the quasi-fermi level immediately after the EBL region [21]. The measured effective barrier height of holes for N-EBL, C-EBL, and W-EBL are 0 meV, 932 meV, and 846 meV. The reduced effective barrier height of the W-EBL compared to the C-EBL improves the hole injection into the active region. Besides, the EBL accelerates the hole by providing kinetic energy, which helps the hole to be distributed across the MQW and obtain a more uniform carrier distribution. A uniform electron-hole distribution may enhance the luminescence intensity of the DUV-LED by several folds [23]. Implementing the EBL improves the confinement and distribution of the carrier in the MQW. The effects of the EBL can be further analyzed via the radiative recombination rates.

## Radiative recombination rates

Radiative recombination can be described as the phenomenon of electrons in the conduction band recombining with the hole in the valance band. The energy loss is released through photons or light emissions [24]. Fig. 3 shows the radiative recombination rates of the DUV-LED in the MQW for N-EBL, C-EBL, and W-EBL, respectively.

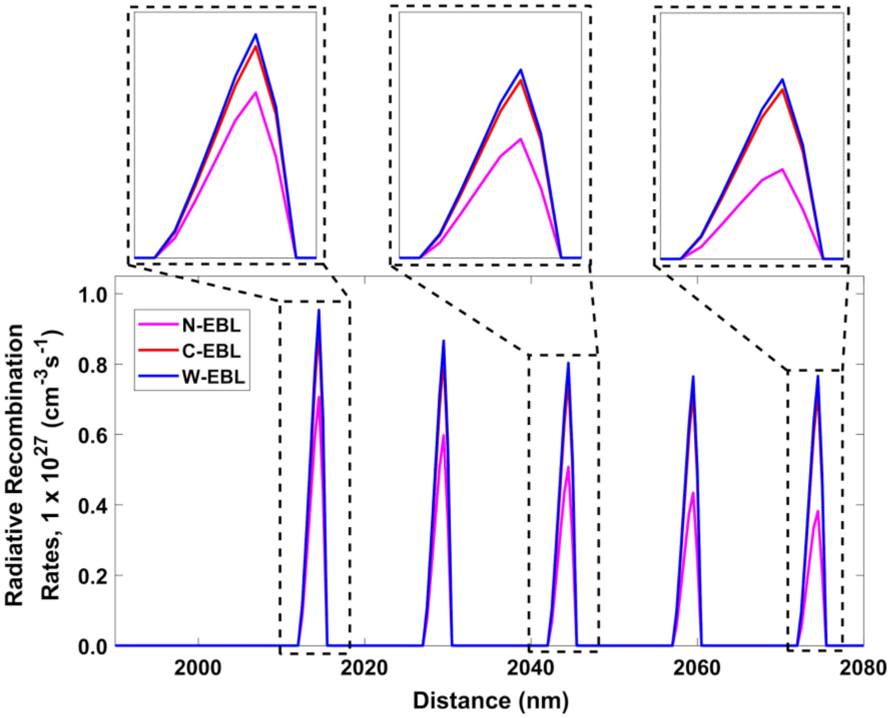


Fig. 3. The radiative recombination rates of the DUV-LED for N-EBL, C-EBL, and W-EBL.

Based on Fig. 3, the radiative recombination rates of the W-EBL are the highest, followed by C-EBL and N-EBL. Furthermore, the importance of the EBL in the DUV-LED has also been highlighted since there is a huge discrepancy in the magnitude of the radiative recombination rates between the N-EBL and C-EBL. The results illustrate that the radiative recombination rates align with the previous analysis in the energy band diagrams. The N-EBL suffers severe electron leakage and low hole confinement in the active region; thus, the radiative recombination rates of the N-EBL are the lowest.

The C-EBL experiences less electron leakage than the N-EBL, and the hole injection into the active region has also improved. Several folds have enhanced the radiative recombination rates of the C-EBL in comparison with the N-EBL. The W-EBL suffers minimal electron leakage and significant improvement in hole confinement in the active region. Due to the hole being appropriately distributed in the MQW for W-EBL, the radiative recombination rates from the first to the fifth quantum well are the highest. Therefore, the W-EBL greatly improved the performance of the optoelectronics properties of the DUV-LED via the increment of the electron and hole confinement [25], [26]. The benefits of obtaining high radiative recombination can be visualized via the luminescence spectrum. Fig. 4 depicts the luminescence spectrum of the DUV-LED and the shifted wavelength due to the implementation of the graded Aluminium composition in the EBL.

## Luminescence spectrum

The photon emission of the DUV-LED can be achieved through the radiative recombination process [24]. By controlling the appropriate amount of the Aluminium composition for the MQW, the desired wavelength emitted by the DUV-LED can be obtained. Each wavelength category has its purpose

https://doi.org/10.24191/scl.v18i4.9714

because the different wavelengths have different frequencies, which may affect the interested applications [27]. Fig. 4 shows the luminescence spectrum of the DUV-LED and the shifted wavelength due to the addition of the EBL.

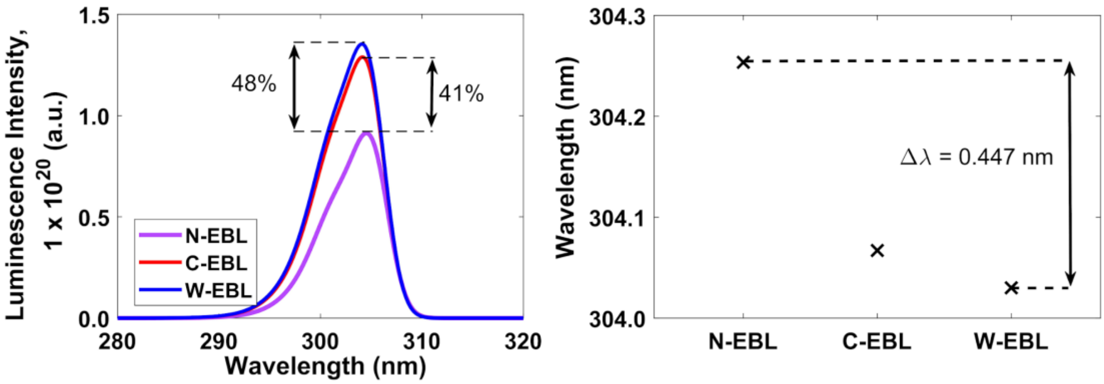


Fig. 4. The a) luminescence spectrum and b) shifted wavelength of the DUV-LED for N-EBL, C-EBL, and W-EBL.

Based on Fig. 4a), the emission of the luminescence intensity for W-EBL and C-EBL has been enhanced by 48% and 41% relative to the N-EBL, respectively. This is attributed to the EBL, which blocks the overflow of the electron from the active region into the p-region and increases the hole injection from the p-region into the active region. Furthermore, the emission wavelengths for N-EBL, C-EBL, and W-EBL are 304.507 nm, 304.134 nm, and 304.06 nm, respectively.

The wavelength emitted by the DUV-LED differs slightly due to the strained quantum well layer, leading to slight bandgap energy changes [28]. The emission of the wavelength depends on the bandgap energy [23]. Thus, any subtle change in the bandgap energy will affect the emitted wavelength. Table 1 shows the summary of this research.

Table 1. The electron and hole barrier height, luminescence intensity, bandgap energy, and wavelength emitted by the N-EBL, C-EBL, and W-EBL DUV-LED structures.

| DUV-LED Structure | Electron Barrier Height (meV) | Hole Barrier Height (meV) | Luminescence Intensity (a.u.) | Bandgap Energy (eV) | Wavelength Emitted (nm) |
|---|---|---|---|---|---|
| N-EBL | 0 | 0 | $0.9133 \times 10^{20}$ | 4.079 | 304.507 |
| C-EBL | 618 | 932 | $1.2891 \times 10^{20}$ | 4.084 | 304.134 |
| W-EBL | 509 | 846 | $1.3531 \times 10^{20}$ | 4.085 | 304.060 |

## CONCLUSION

In conclusion, the N-EBL, C-EBL, and W-EBL of DUV LED were analyzed based on the energy band diagrams, radiative recombination rates, and luminescence spectrum. The EBL was used to block the electron overflow and improve hole injection in the MQW. The EBL analysis achieved an optimal effective carrier barrier height, and the luminescence intensity of the DUV-LED was boosted two-fold. Besides, the grading of the EBL via aluminium composition also affects the carrier transportation in the epilayer and the optoelectronics performances. Considering the N-EBL as a reference, the luminescence intensity of the W-EBL, which was enhanced via grading the aluminum composition, was higher than that of the N-EBL and C-EBL by 48% and 8%, respectively. Moreover, the addition of EBL in the epilayer slightly influences the wavelength emitted by the DUV-LED. However, its shift was insignificant because the wavelength is

https://doi.org/10.24191/scl.v18i4.9714

still in the range of 304 nm. Therefore, this research provides new insights into the EBL configurations in the AlGaN-based DUV-LED epilayer.

## ACKNOWLEDGEMENTS/FUNDING

The authors would like to acknowledge the support of CAPTOR, IPQC, and the Department of Physics, International Islamic University Malaysia, in terms of facilities and financial by the Ministry of Education (Malaysia) through the Fundamental Research Grant Scheme (Project No.: FRGS 19-033-0641) (References No.: FRGS/1/2018/TK07/UIAM/02/1).

## CONFLICT OF INTEREST STATEMENT

The authors agree that this research was conducted without any self-benefits or commercial or financial conflicts and declare the absence of conflicting interests with the funders.

## AUTHORS' CONTRIBUTIONS

Mohammad Amirul Hairol Aman conceived the original idea, conceptualized the research idea, carried out the research, designed it, and wrote the article. Nurul Fathinah Azrisham wrote the article. Ahmad Nadzimuddin Nazmi wrote the article. Ahmad Fakhrurrazi Ahmad Noorden supervised the research progress, anchored the review, and revised and approved the article submission.

## REFERENCES

[1] Kumar, L. R., Yellapu, S. K., Tyagi, R. D., & Zhang, X. (2019). A review on variation in crude glycerol composition, bio-valorization of crude and purified glycerol as carbon source for lipid production. *Bioresource Technology, 293*, Article 122155. https://doi.org/10.1016/j.biortech.2019.122155

[2] Ayoub, M., & Abdullah, A. Z. (2012). Critical review on the current scenario and significance of crude glycerol resulting from biodiesel industry towards more sustainable renewable energy industry. *Renewable and Sustainable Energy Reviews, 16*(5), 2671–2686. https://doi.org/10.1016/j.rser.2012.01.054

[3] Aziz, A., Raman, A., Tan, H. W., & Buthiyappan, A. (2019). Two-step purification of glycerol as a value-added byproduct from the biodiesel production process. *Frontiers in Chemistry, 7*, Article 774. https://doi.org/10.3389/fchem.2019.00774

[4] Hájek, M., & Skopal, F. (2010). Treatment of glycerol phase formed by biodiesel production. *Bioresource Technology, 101*(9), 3242–3245. https://doi.org/10.1016/j.biortech.2009.12.094

[5] Manosak, R., & Limpattayanate, S. (2011). Sequential-refining of crude glycerol derived from waste used-oil methyl ester plant via a combined process of chemical and adsorption. *Fuel Processing Technology, 92*(1), 92–99. https://doi.org/10.1016/j.fuproc.2010.09.002

[6] Hunsom, M., & Autthanit, C. (2013). Adsorptive purification of crude glycerol by sewage sludge-derived activated carbon prepared by chemical activation with $H_3PO_4$, $K_2CO_3$, and KOH. *Chemical Engineering Journal, 229*, 334–343. https://doi.org/10.1016/j.cej.2013.05.120

[7] Fairous, S., Rusnah, S., & Maryam, H. (2010). Potential source of biofuel from pyrolysis of treated sewage sludge. *CSSR 2010 - 2010 International Conference on Science and Social Research*, 1272–1277. https://doi.org/10.1109/CSSR.2010.5773732

[8] Baru, P. A., & Hassan, S. (2018). Characterization of Malaysian sewage sludge dried using thermal dryer. *Journal of Engineering and Applied Sciences, 5*(1), 24–29.

[9] Chenyu, W., Xiaolong, L., Weibo, S., Xiaohui, S., & Chao, H. (2023). Elaboration of cost-effective adsorbents derived from sewage sludge through hydrothermal carbonization: Influence of process

parameters and feedstock components on the adsorption performance. *Journal of Cleaner Production, 434*, Article 140358. https://doi.org/10.1016/j.jclepro.2023.140358

[10] Xiaoyang, Y., Baofeng, W., & Fangqin, C. (2024). Adsorption performance on tetracycline by novel magnetic adsorbent derived from hydrochar of low-rank coal and sewage sludge. *Separation and Purification Technology, 330*, Article 125482. https://doi.org/10.1016/j.seppur.2023.125482

[11] Eleonora, S., Sandra, V., Nicola, D. F., & Monica, P. (2023). Tailoring the porosity of chemically activated carbons derived from the HTC treatment of sewage sludge for the removal of pollutants from gaseous and aqueous phases. *Journal of Environmental Management, 345*, Article 118887. https://doi.org/10.1016/j.jenvman.2023.118887

[12] Zhai, Y., Wei, X., & Zeng, G. (2004). Effect of pyrolysis temperature and hold time on the characteristic parameters of adsorbent derived from sewage sludge. *Journal of Environmental Sciences, 16*(4), 683–686.

[13] Bandosz, T. J., & Block, K. (2006). Municipal sludge-industrial sludge composite desulfurization adsorbents: Synergy enhancing the catalytic properties. *Environmental Science & Technology, 40*(10), 3378–3383. https://doi.org/10.1021/es052272d

[14] Smith, K. M., Fowler, G. D., Pullket, S., & Graham, N. J. D. (2009). Sewage sludge-based adsorbents: A review of their production, properties, and use in water treatment applications. *Water Research, 43*(10), 2569–2594. https://doi.org/10.1016/j.watres.2009.02.038

[15] Kutty, S. R. M., Almahbashi, N. M. Y., Nazrin, A. A. M., Malek, M. A., Noor, A., Baloo, L., & Ghaleb, A. A. S. (2019). Adsorption kinetics of colour removal from palm oil mill effluent using wastewater sludge carbon in column studies. *Heliyon, 5*(10), e02439. https://doi.org/10.1016/j.heliyon.2019.e02439

[16] Abbas, M., Zaini, A., Zakaria, M., & Mohd, S. H. (2013). Sludge-adsorbents from palm oil mill effluent for methylene blue removal. *Journal of Environmental Chemical Engineering, 1*(4), 1091–1098. https://doi.org/10.1016/j.jece.2013.08.026

[17] Devi, P., & Saroha, A. K. (2016). Improvement in performance of sludge-based adsorbents by controlling key parameters by activation/modification: A critical review. *Critical Reviews in Environmental Science and Technology, 46*(24), 3389–3444. https://doi.org/10.1080/10643389.2016.1260902

[18] Zahoor, M. (2011). Effect of agitation speed on adsorption of imidacloprid on activated carbon. *Journal of the Chemical Society of Pakistan, 33*(3), 305–312.

[19] Environ, J. (2016). Decolorization of basic textile dyes using a novel adsorbent modification method: Ultrasonic-acid modification. *Environmental Science and Pollution Research, 10*(1), 31–40.

[20] Gorzin, F., & Bahri Rasht Abadi, M. M. (2018). Adsorption of Cr(VI) from aqueous solution by adsorbent prepared from paper mill sludge: Kinetics and thermodynamics studies. *Adsorption Science & Technology, 36*(1–2), 149–169. https://doi.org/10.1177/0263617416686976

[21] Kuang, Y., Zhang, X., & Zhou, S. (2020). Adsorption of methylene blue in water onto activated carbon by surfactant modification. *Water, 12*(2), 1–19. https://doi.org/10.3390/w12020587

[22] Tsai, W. T., Lai, C. W., & Hsien, K. J. (2003). Effect of particle size of activated clay on the adsorption of paraquat from aqueous solution. *Journal of Colloid and Interface Science, 263*(1), 29–34. https://doi.org/10.1016/S0021-9797(03)00213-3

[23] Aljeboree, A. M., Alshirif, A. N., & Alkaim, A. F. (2014). Kinetics and equilibrium study for the adsorption of textile dyes on coconut shell activated carbon. *Arabian Journal of Chemistry, 10*, S3381–S3393. https://doi.org/10.1016/j.arabjc.2014.01.020

[24] Vaverde, A., Cabrera-Codony, A., Calvo-Schwarzwalder, M., & Myers, T. G. (2024). Investigating the impact of adsorbent particle size on column adsorption kinetics through a mathematical model. *International Journal of Heat and Mass Transfer, 218*, Article 124724. https://doi.org/10.1016/j.ijheatmasstransfer.2023.124724